Eur. Phys. J. A **26**, 201–207 (2005)
DOI 10.1140/epja/i2005-10165-4

THE EUROPEAN PHYSICAL JOURNAL A

Effective three-body interactions in the α-cluster model for the ^{12}C nucleus

S.I. Fedotov, O.I. Kartavtsev[a], and A.V. Malykh

Joint Institute for Nuclear Research, Dubna, 141980, Russia

Received: 9 September 2005 / Revised version: 13 October 2005 /
Published online: 1 December 2005 – © Società Italiana di Fisica / Springer-Verlag 2005
Communicated by G. Orlandini

Abstract. Properties of the lowest 0^+ states of ^{12}C are calculated to study the role of three-body interactions in the α-cluster model. An additional short-range part of the local three-body potential is introduced to incorporate the effects beyond the α-cluster model. There is enough freedom in this potential to reproduce the experimental values of the ground-state and excited-state energies and the ground-state root-mean-square radius. The calculations reveal two principal choices of the two-body and three-body potentials. Firstly, one can adjust the potentials to obtain the width of the excited 0_2^+ state and the monopole $0_2^+ \to 0_1^+$ transition matrix element in good agreement with the experimental data. In this case, the three-body potential has strong short-range attraction supporting a narrow resonance above the 0_2^+ state, the excited-state wave function contains a significant short-range component, and the excited-state root-mean-square radius is comparable to that of the ground state. Next, rejecting the solutions with an additional narrow resonance, one finds that the excited-state width and the monopole transition matrix element are insensitive to the choice of the potentials and both values exceed the experimental ones.

PACS. 21.45.+v Few-body systems – 21.60.Gx Cluster models – 23.60.+e α decay – 24.30.Gd Other resonances

1 Introduction

As the α-particle is the most tightly bound nucleus, a variety of the low-energy nuclear properties can be successfully described within the framework of the α-cluster model. The effective two-body and, for more than two α-particles, at least three-body potentials must be determined as an input for the model. The three-body calculations allow one to reduce the ambiguity in the two-body potential which could not be determined merely from the two-body data. In this respect, the basic problem is to check the model for the system of three α-particles, thus, the effective potentials should be chosen by fitting the main characteristics of the ^{12}C nucleus to the experimental values.

In spite of significant simplifications provided by the α-cluster model, there are complicated problems inherent in the processes with few charged particles in the initial or final state. For problems of this kind the main difficulty stems from the necessity to describe the continuum wave function, and even the qualitative understanding of the reaction mechanism is crucial. The formation of the ^{12}C nucleus in the triple-α low-energy collisions, which plays a key role in stellar nucleosynthesis [1,2], is a well-known example. More examples are the double-proton radioactivity, which has been a subject of thorough experimental and theoretical investigations during the last few years (for details see the recent reviews [3,4]), and the decay of the long-lived $^{12}\mathrm{C}(1^+)$ state [5]. Note also a description of the multicluster decay of atomic nuclei by using the quasi-classical approach to Coulomb-correlated penetration through a multidimensional potential barrier [6].

In the triple-α reaction both the low-energy α-α resonance (the ground state of ^{8}Be) and the near-threshold three-body resonance ($^{12}\mathrm{C}(0_2^+)$ state) play an important role. These resonances are predicted in ref. [2] as the unique possibility for helium burning that provides the only explanation for the observable abundance of elements in the Universe. Due to these resonances, the triple-α reaction in stars goes through the sequential reaction $3\alpha \to {}^8\mathrm{Be} + \alpha \to {}^{12}\mathrm{C}(0_2^+) \to {}^{12}\mathrm{C} + \gamma$. The predicted $^{12}\mathrm{C}(0_2^+)$ state, starting with observation [7,8], was thoroughly studied later on, in particular, the decay mechanism was investigated in ref. [9].

Among other interesting problems connected with the description of α-cluster nuclei, one should mention the nonresonance reaction $3\alpha \to {}^{12}\mathrm{C}$, which is responsible for helium burning at ultra-low temperatures and high densities as it occurs in accretion of helium on white dwarfs and

[a] e-mail: oik@nusun.jinr.ru

neutron stars [10]. Whereas a number of model calculations of the nonresonance reaction are available [11–14], a consistent three-body description is needed to avoid a possible error of a few orders of magnitude in the calculated reaction rate. Note also that recently the α-cluster states in nuclei have attracted attention in connection with the problem of α-particle condensation (see, *e.g.*, ref. [15] and references therein).

The focus of the present paper is to shed light, using the technique of ref. [16], on the role of the three-body interactions in the description of the lowest 0^+ states of ^{12}C. The main question to be answered is to what extent the α-cluster model is able to reproduce the experimental energies and sizes of the nuclear states. The next more challenging problem is to describe the fine characteristics, such as the width of the near-threshold 0_2^+ state and $0_2^+ \to 0_1^+$ monopole transition matrix element (MTME), which are sensitive to the choice of the potentials. In realistic calculations, the finite size of the α-particle implies the crucial importance of the effective three-body interactions for a reliable description within the framework of the α-cluster model [16–18]. Furthermore, the effective three-body interactions could be used to take into account the non–α-cluster structure of the nucleus at short distances in addition to the effect of α-particle distortions at large distances. Clearly, the choice of the effective two-body and three-body potentials must be governed by the results of the three-body calculations aimed at an optimal description of the ^{12}C characteristics.

2 Theoretical background

The present paper is aimed at choosing, by means of microscopic three-body calculations of the ground and first-excited 0^+ states of ^{12}C, the effective three-body and two-body potentials of the α-cluster model. It is assumed that all the effects connected with both the internal structure of α-particles and the identity of nucleons are incorporated in the effective potentials. In particular, the three-body potential is chosen to include the short-range effects of antisymmetrization in the 12-nucleon system, which are not taken into account by the two-body potential. The two-body input is defined by the local α-α potential that reproduces the experimental energy and width of the near-threshold α-α resonance (ground state of ^{8}Be). More precisely, with the ^{8}Be energy fixed and its width varying within the experimental uncertainty, a set of two-body potentials is constructed by modification of the Ali-Bodmer s-wave potential [19]. One uses a simple, and suitable for calculation, functional form of the three-body potential, which depends only on the collective variable, *viz*, the hyper-radius. A sum of two Gaussian terms is used, which makes it possible to take into account both the effect of α-particle distortions at large distances and the short-range non–α-cluster effects. Calculation of the resonance width and the MTME makes sense only if, not only the ground-state energy, but also the resonance position and the root-mean-square (r.m.s.) radius of the ground state are fixed at the experimental values. These requirements are satisfied by adjusting the parameters of the three-body potential.

The technical details and the numerical procedure are basically the same as in the previous paper [16]; therefore, only a sketch of the calculational method will be given below. The method is based on the expansion of the total wave function in terms of the eigenfunctions on a hypersphere [20]. The eigenvalue problem on a hypersphere is numerically solved by using the variational method.

The units $\hbar = m = e = 1$ are used throughout the paper unless otherwise specified. The scaled Jacobi coordinates are defined as $\mathbf{x}_i = \mathbf{r}_j - \mathbf{r}_k$, $\mathbf{y}_i = (2\mathbf{r}_i - \mathbf{r}_j - \mathbf{r}_k)/\sqrt{3}$, where the indices $\{ijk\}$ must be chosen as a permutation of $\{123\}$ and $\mathbf{r}_i$ is the position vector of the i-th particle. The hyperspherical variables ρ, α_i, and θ_i, are defined via the Jacobi coordinates by the relations $x_i = \rho\cos\frac{\alpha_i}{2}$, $y_i = \rho\sin\frac{\alpha_i}{2}$, and $\cos\theta_i = \frac{(\mathbf{x}_i\cdot\mathbf{y}_i)}{x_i y_i}$.

The Schrödinger equation for three α-particles is

$$\left(-\Delta_{\mathbf{x}} - \Delta_{\mathbf{y}} + \sum_{j=1}^{3} V(x_j) + V_3(\rho) - E \right)\Psi = 0 \ , \qquad (1)$$

where the total interaction contains the pair-wise potentials $V(x_i)$ and the three-body potential $V_3(\rho)$. The two-body potential is a sum $V(x) = V_s(x) + V_c(x)$, where

$$V_s(x) = V_r e^{-\mu_r^2 x^2} - V_a e^{-\mu_a^2 x^2} \qquad (2)$$

and $V_c(x) = \dfrac{4}{x}$. The three-body potential is taken as an obvious extension of the potential used in refs. [16–18],

$$V_3(\rho) = V_0 e^{-(\rho/b_0)^2} + V_1 e^{-(\rho/b_1)^2} \ . \qquad (3)$$

With the expansion of the total wave function

$$\Psi = \rho^{-5/2} \sum_n f_n(\rho)\Phi_n(\alpha,\theta,\rho) \qquad (4)$$

in a series of the normalized eigenfunctions Φ_n satisfying the equation

$$\left[\frac{\partial^2}{\partial\alpha^2} + 2\cot\alpha\frac{\partial}{\partial\alpha} + \frac{1}{\sin^2\alpha}\left(\frac{\partial^2}{\partial\theta^2} + \cot\theta\frac{\partial}{\partial\theta} \right) - \frac{\rho^2}{4}\sum_{j=1}^{3} V\left(\rho\cos\frac{\alpha_j}{2}\right) + \lambda_n(\rho) \right]\Phi_n(\alpha,\theta,\rho) = 0 \ , \qquad (5)$$

the Schrödinger equation (1) is routinely transformed to the system of hyper-radial equations (HRE),

$$\left[\frac{\partial^2}{\partial\rho^2} - \frac{1}{\rho^2}\left(4\lambda_n(\rho) + \frac{15}{4} \right) - V_3(\rho) + E \right] f_n(\rho) + \sum_m \left(Q_{nm}(\rho)\frac{\partial}{\partial\rho} + \frac{\partial}{\partial\rho}Q_{nm}(\rho) - P_{nm}(\rho) \right) f_m(\rho) = 0 \ , \qquad (6)$$

$$Q_{nm}(\rho) = \left\langle \Phi_n \,\middle|\, \frac{\partial\Phi_m}{\partial\rho} \right\rangle , \quad P_{nm}(\rho) = \left\langle \frac{\partial\Phi_n}{\partial\rho} \,\middle|\, \frac{\partial\Phi_m}{\partial\rho} \right\rangle , \qquad (7)$$

where $\langle\cdot|\cdot\rangle$ stands for integration on the hypersphere.

The functions $\lambda_n(\rho)$, $Q_{nm}(\rho)$, and $P_{nm}(\rho)$ are calculated by using the variational solutions of the eigenvalue problem (5). In view of the symmetry of $\Phi_n(\alpha,\theta,\rho)$, which follows from the identity of α-particles, the variational trial functions are chosen to be symmetric under any permutation of particles. Few types of trial functions are used, which provides flexibility of the variational basis needed to describe an essentially different structure of the wave function at different values of ρ, in particular, the two- and three-cluster configurations in the asymptotic region. Thus, the variational basis contains a set of the symmetric hyperspherical harmonics which are eigenfunctions of the differential operator in eq. (5). Furthermore, to describe the two-cluster configuration, symmetrized combinations of the ρ-dependent two-body functions $\phi_i(x)$ are included in the basis. As in ref. [16], a set of $\phi_i(x)$ includes Gaussian functions $\phi_i(x) = \exp(-\beta_i x^2)$, which allows the two-cluster wave function to be described within the range of the nuclear potential $V_s(r)$, and the function $\phi(x) = x^{1/4}\exp(-4\sqrt{x}(1+ax))$ to describe the two-cluster wave function in the sub-barrier region.

Solutions of the eigenvalue problem (at $E<0$) and the $\alpha+{}^8$Be scattering problem (at $E>0$) for HRE (6) provide the properties of the ground 0_1^+ state and the excited 0_2^+ resonance state, respectively. The resonance position E_r and width Γ are determined by fitting the phase shift δ_E for $\alpha+{}^8$Be scattering to the Wigner dependence on energy,

$$\cot(\delta_E - \delta_{bg}) = \frac{2}{\Gamma}(E_r - E)\ , \qquad (8)$$

where δ_E is defined by the asymptotic form of the first-channel radial function $f_1(\rho)$ (see eq. (23) in ref. [16]) and the background phase shift δ_{bg} is of no interest for the present calculation. It is suitable to treat the ultra-narrow 0_2^+ resonance state on equal footing with the ground state. Therefore, its wave function, defined as the scattering solution at the resonance energy E_r, is normalized on the finite interval $0 \le \rho \le \rho_t$, where ρ_t is the turning point of the first-channel hyper-radial potential $U_1(\rho) = \frac{1}{\rho^2}\left(4\lambda_1(\rho)+\frac{15}{4}\right)+V_3(\rho)+P_{11}(\rho)$. Thus, the r.m.s. radii $R^{(i)}$ of the ground ($i=1$) and excited ($i=2$) states and MTME M_{12} are defined by the expressions

$$R^{(i)} = \sqrt{R_\alpha^2 + \frac{1}{6}\bar{\rho}_i^2}\ , \qquad \bar{\rho}_i^2 = \sum_n \int_0^\infty \left|f_n^{(i)}(\rho)\right|^2 \rho^2 \mathrm{d}\rho\ , \quad (9)$$

where $R_\alpha = 1.47$ fm is the r.m.s. radius of the α-particle, and

$$M_{12} = \sum_n \int_0^{\rho_t} f_n^{(2)}(\rho) f_n^{(1)}(\rho)\rho^2 \mathrm{d}\rho\ . \qquad (10)$$

3 Results

Calculations have been performed with a family of the two-body α-α potentials V_s (2), which are obtained by modification of potential (a) from ref. [19]. With the ranges of the repulsive and attractive parts fixed at the values $\mu_r^{-1} = 1.53$ fm and $\mu_a^{-1} = 2.85$ fm, the parameters V_r and V_a were chosen to reproduce the experimental energy $E_{2\alpha} = 91.89$ keV [21] of the α-α resonance (ground state of ^{8}Be) and to vary its width within the experimental uncertainty $\gamma = 6.8 \pm 1.7$ eV [21]. As the width γ unambiguously determines the parameters of the two-body potential, in the following the potential will be marked by γ. A partial set of the parameters V_r and V_a and the widths γ is presented in table 1. For all the potentials under consideration, the calculation of the s-wave α-α scattering shows a similar dependence of the phase shifts on energy. In fact, the phase shifts multiplied by a proper factor coincide for different potentials up to an energy of about 7 MeV. The best agreement of the calculated phase shifts with experimental data is obtained for the potential with $\gamma = 6.8$, whereas the phase shifts calculated with other potentials are scaled by the factor C presented in table 1.

Table 1. Parameters of the α-α potential V_s (2) providing the α-α resonance widths γ. The meaning of the factor C is described in the text.

γ (eV)	V_r (MeV)	V_a (MeV)	C
5.69	35.024	19.492	1.135
6.20	52.772	22.344	1.07
6.37	60.051	23.359	1.05
6.40	61.220	23.516	1.045
6.50	66.028	24.141	1.03
6.60	71.057	24.766	1.02
6.80	82.563	26.1	1.0

The three-channel system of HREs (6) is solved to calculate the ground- and excited-state energies E_{gs} and E_r, the r.m.s. radii $R^{(i)}$, the excited-state width Γ, and the monopole transition matrix element M_{12}. Convergence in a number of HREs is sufficiently fast and the solution of three HREs allows the resonance width to be determined with an accuracy not worse than 1 eV. Generally, the parameters of the numerical procedure and an accuracy of the calculated E_{gs}, E_r, Γ, $R^{(i)}$, and M_{12} were the same as in ref. [16]. Using the numerical procedure of determination of E_{gs}, E_r, and $R^{(1)}$, the parameters of the three-body potential for each two-body potential were determined by solving the nonlinear inverse problem of fixing the ground- and excited-state energies and the ground-state r.m.s. radius at the experimental values $E_{gs} = -7.2747$ MeV, $E_r = 0.3795$ MeV [22], and $R^{(1)}_{exp} = 2.48 \pm 0.22$ fm [23,24].

In starting the description of the results, it is useful to digress into the discussion of the calculations with the one-term three-body potential ($V_1 = 0$), which provide better understanding of the dependence on the three-body potential $V_3(\rho)$. For this two-parameter potential, only E_{gs} and E_r are fixed at the experimental values to determine V_0 and b_0. The calculation gives two types of solutions, that is, two families of one-term three-body potentials, whose parameters V_0 and b_0 are presented in table 2. For one type of solutions, three-body potentials are rather extended with the range about $b_0 = 4.5$ fm and strength $|V_0| < 40$ MeV. The ground-state r.m.s. radius

Table 2. Two families of solutions with the one-term three-body potential ($V_1 = 0$) for a number of two-body potentials marked by the widths γ (eV) of the α-α resonance. Shown are the parameters b_0 (fm) and V_0 (MeV), the r.m.s. radii $R^{(i)}$ (fm), the width of the excited state Γ (eV), and the monopole transition matrix element M_{12} (fm^2).

γ	b_0	V_0	Γ	$R^{(1)}$	$R^{(2)}$	M_{12}	b_0	V_0	Γ	$R^{(1)}$	$R^{(2)}$	M_{12}
5.69	4.5001	−18.600	13.0	2.35	3.7	8.59	2.2310	−89.941	8.2	2.02	3.4	6.46
6.20	4.6006	−20.824	15.9	2.45	3.8	8.87	2.3314	−113.28	9.7	2.09	3.5	6.90
6.37	4.6247	−21.643	16.9	2.48	3.9	8.93	2.3472	−125.05	10.2	2.12	3.5	7.01
6.40	4.6455	−21.640	17.2	2.48	3.9	8.97	2.3464	−127.48	10.4	2.12	3.5	7.03
6.50	4.6379	−22.297	17.6	2.50	3.9	8.97	2.3547	−135.38	10.7	2.13	3.5	7.09
6.60	4.6455	−22.838	18.1	2.51	3.9	8.99	2.3584	−144.47	11.0	2.14	3.6	7.13
6.80	4.6531	−24.047	19.3	2.55	4.0	9.03	2.3611	−166.39	11.7	2.17	3.6	7.22

is in the range 2.2 fm $< R^{(1)} <$ 2.8 fm, which includes the experimental value, whereas Γ and M_{12} significantly exceed the experimental values $\Gamma = 8.5 \pm 1.0$ eV and $M_{12} = 5.48 \pm 0.22$ fm^2 [22]. For another type of solutions, b_0 is about twice as small and $|V_0|$ exceeds 80 MeV. The ground-state r.m.s. radius is lower than $R^{(1)}_{exp}$; nevertheless, Γ and M_{12} are in better agreement with experiment than in the previous case. As the ground-state size $R^{(1)}$ cannot be fixed at the experimental value by using the one-term three-body potential, it is not surprising that finer properties Γ and M_{12} vary in a wide range with variations of the two-body potential.

The results for the one-term potential ($V_1 = 0$) clearly show lack of simultaneous description for the ground-state size $R^{(1)}$ and the excited-state characteristics Γ and M_{12}. As far as it does not seem reasonable to improve the agreement between calculation and experiment for the very fine properties Γ and M_{12} at the expense of the ground-state r.m.s. radius, one concludes that the one-term three-body potential is too simple to describe the real nucleus. One can readily propose to use simultaneously both the short-range and the long-range term in the three-body potential to obtain a compromise description of the ground-state and excited-state characteristics.

After the digression on the one-term three-body potential, one returns to the main route of the calculations with the two-term $V_3(\rho)$ in the form (3). Four parameters of the three-body potential are used to fix the basic properties, *viz*, the ground-state and excited-state energies and the ground-state r.m.s. radius at the experimental values[1]. Varying one remaining degree of freedom in the four-dimensional space of parameters $V_{0,1}$, $b_{0,1}$ of the three-body potential, one obtains a one-parameter set of solutions, which is suitably represented for each two-body potential by a line in the (Γ, M_{12})-plane, as shown in fig. 1. It turns out that some of the calculated potentials, namely, those for which the parameter $b_0 > 6$ fm, are of the form of a shallow well with a long tail. These solutions of unreasonably long range were withdrawn from consideration and will not be presented.

Furthermore, the parameters of the long-range term in the three-body potential $V_0 \approx 20$ MeV and $b_0 \approx 4.5$ fm

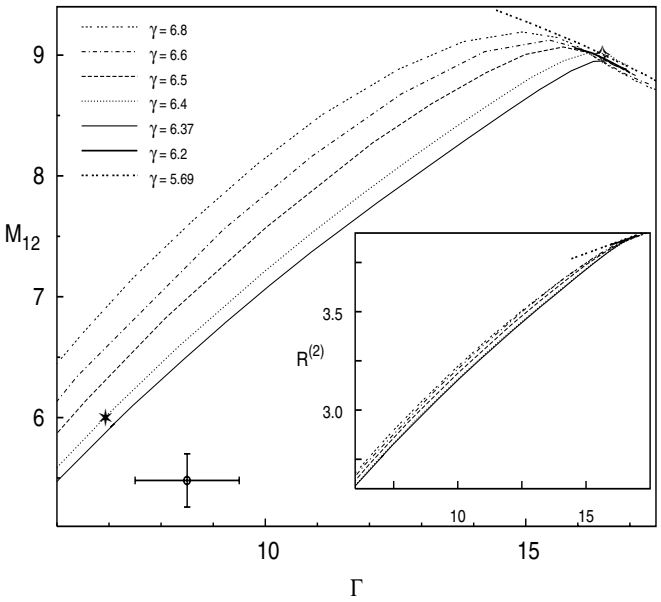

Fig. 1. Calculated M_{12}-Γ relations. Each line depicts the result for the two-body potential marked by the two-body resonance width γ. The point with error bars shows the experimental data. The corresponding $R^{(2)}$-Γ relations are shown in the inset.

are similar to those found in the calculations with the one-term potential. Thus, the long-range tails of the four-parameter three-body potentials and one of the one-term potentials practically coincide. On the other hand, the one-term potentials of another type look like an average of the full three-body potentials at short distances. These qualitative features are seen in fig. 2, where the first-channel hyper-radial potentials $U_1(\rho)$ are presented.

All the solutions turn out to pass through a small common area about $\Gamma \approx 16.5$ eV and $M_{12} \approx 9$ fm^2, which is marked by a diamond in fig. 1. This area is well separated from the experimental values. Correspondingly, the calculated values of the excited-state r.m.s. radius are concentrated around the value $R^{(2)} \approx 3.9$ fm. This surprising insensitivity of Γ, M_{12}, and $R^{(2)}$ to the choice of the two-body and three-body potentials results from the imposed requirement to fix the ground-state r.m.s. radius at the experimental value.

[1] In the present calculation, the ground-state r.m.s. radius $R^{(1)}$ is fixed at the elder experimental value of 2.47 fm [25] that does not reflect on the conclusions.

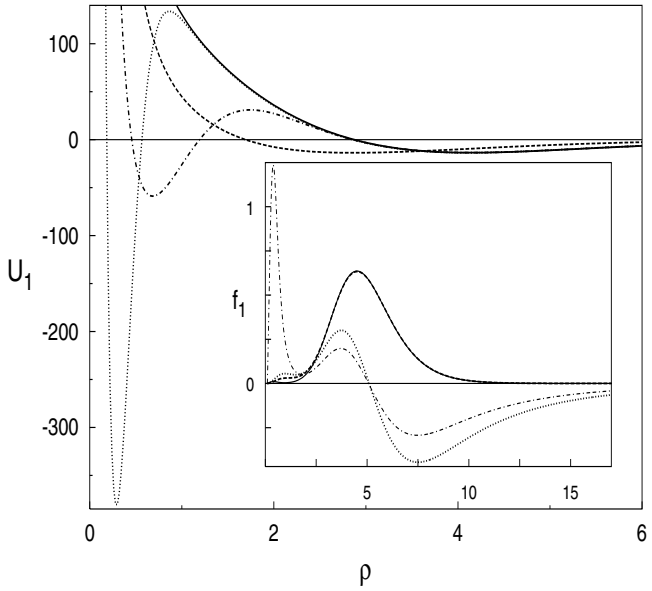

Fig. 2. The first-channel hyper-radial potentials $U_1(\rho)$ calculated for the two-body potential providing $\gamma = 6.4$ eV. Dash-dotted and dotted lines depict $U_1(\rho)$ for the three-body potentials whose parameters are marked in table 3 by a diamond and an asterisk, respectively. Full and dashed lines depict $U_1(\rho)$ for the one-term three-body potential whose parameters are given in line 4 of table 2. The inset shows the first-channel radial functions $f_1(\rho)$ for the potential marked by an asterisk (full and dash-dotted lines for the ground and excited states) and for the potential marked by a diamond (dashed and dotted lines for the ground and excited states).

The solutions could be separated into two classes, which are characterized by the sign of the short-range term in the three-body potential. The solutions of the first class ($V_1 < 0$) are found for $\gamma > 6.35$ eV and those of the second class ($V_1 > 0$) for $\gamma < 6.35$ eV. Note that this separation is correlated with the dependence of the ground-state r.m.s. radius $R^{(1)}$ on γ found in the above calculations for the extended one-term potentials. If $R^{(1)} < R^{(1)}_{exp}$, which takes place for $\gamma < 6.35$ eV, one needs to add a repulsive term ($V_1 > 0$), and if $R^{(1)} > R^{(1)}_{exp}$ (for $\gamma > 6.35$ eV), an attractive term must be added to fix $R^{(1)}$ at the experimental value. For the second-class solutions, the larger Γ the smaller M_{12}; therefore, the corresponding lines never approach the experimental data. On the contrary, for the solutions of the first class ($\gamma > 6.35$ eV), the lines in the (Γ, M_{12})-plane bend downward inside the common area that provides an option to diminish simultaneously Γ and M_{12}.

More detailed consideration of the dependence on the two-body potential (on the parameter γ) shows that the lines in the (Γ, M_{12})-plane representing the solutions of the first class form a band, as seen in fig. 1. The upper and lower borders of the band correspond to $\gamma \approx 6.8$ eV and $\gamma \approx 6.35$ eV, respectively. The dependence on γ (for $\gamma > 6.8$ eV) becomes weak so that the lines in the (Γ, M_{12})-plane are rather close to the upper border,

Table 3. Parameters of the three-body potential and characteristics of the ^{12}C(0^+) states. The two-body potential provides the α-α resonance width $\gamma = 6.4$ eV. An asterisk and a diamond mark two solutions which are also depicted in fig. 1.

	V_0 (MeV)	b_0 (fm)	V_1 (MeV)	b_1 (fm)	Γ (eV)	M_{12} (fm^2)	$R^{(2)}$ (fm)
$\diamond$	-22.189	4.5699	-411.719	1.0155	16.5	9.01	3.86
$*$	-22.867	4.5109	-1710.00	0.41009	7.0	6.0	2.76

though being inside the band. For decreasing γ below 6.8 eV, the lines in the (Γ, M_{12})-plane shift downward until the critical value about $\gamma \approx 6.35$ eV is reached. An abrupt transition to the second-class solutions takes place at the critical value of γ, beyond which the lines in the (Γ, M_{12})-plane always remain near the common area ($\Gamma \approx 16.5$ eV, $M_{12} \approx 9$ fm^2). The dependence of $R^{(2)}$ on γ is illustrated in the inset in fig. 1, where it is seen that for $\gamma > 6.35$ eV the lines lie within a narrow band in the $(\Gamma, R^{(2)})$-plane. Alternatively, for $\gamma < 6.35$ eV, the calculated values are in a small area about $\Gamma \approx 16.5$ eV and $R^{(2)} \approx 3.9$ fm.

The described features are closely connected with the form of the three-body potential, in particular, the smaller Γ, M_{12}, and $R^{(2)}$ the larger the strength $|V_1|$ of the attractive term and the smaller its range b_1. To exemplify these considerations, let us consider a typical two-body potential with $\gamma = 6.4$ eV and a particular three-body potential, which gives Γ and M_{12} (marked by an asterisk in fig. 1) sufficiently close to the experimental data. The parameters of the three-body potential, Γ, M_{12}, and $R^{(2)}$ at this point are compared in table 3 with the corresponding values, which are typical of the common area (marked by a diamond). The excited-state r.m.s. radius $R^{(2)}$, as shown in the inset in fig. 1, decreases with decreasing Γ from the typical value $R^{(2)} \approx 3.9$ fm for solutions near the common area to $R^{(2)} \approx 2.8$ fm for solutions near the point marked by an asterisk that only slightly exceeds the ground-state r.m.s. radius $R^{(1)} = 2.47$ fm. The diminishing of $R^{(2)}$ to these small values underlines a comparatively compact structure of the excited state. Indeed, the excited-state wave functions, as shown in the inset in fig. 2, are quite different for the solutions marked by a diamond and an asterisk. Nevertheless, the ground-state wave functions are surprisingly similar to each other.

A drastic modification of the excited-state wave function at short distances for the solution with small Γ and M_{12} hints that the short-range attractive well in the three-body potential is able to support a near-lying resonance state. Indeed, the calculations reveal an additional resonance, whose energy changes from about 0.5 MeV for the solutions with small Γ and M_{12} to about 1 MeV for the solutions providing Γ and M_{12} near the common area. Correspondingly, the resonance width increases from hundreds of eV up to hundreds of keV. In particular, considering the two-body potential with $\gamma = 6.4$ eV, one finds that energy and width of the additional resonance increase from $E^* = 0.48$ MeV and $\Gamma^* = 0.26$ keV (for the three-body potential with $\Gamma = 7$ eV) to $E^* = 1.12$ MeV

and $\Gamma^* = 34.4$ keV (for the three-body potential with $\Gamma = 15.2$ eV).

4 Summary and discussion

The lowest 0^+ states of ^{12}C are calculated to study the role of the three-body interactions in the α-cluster model. The method used in the present paper provides an accurate calculation of fine characteristics of ^{12}C, *viz*, the extremely narrow width Γ of the 0^+_2 state and the $0^+_2 \to 0^+_1$ MTME M_{12}. The two-body potentials, obtained by modification of the Ali-Bodmer potential, provide the exact energy of the α-α resonance (the ^{8}Be nucleus), while its width is allowed to vary within the experimental uncertainty. A simple two-Gaussian form of the three-body potential is chosen under the assumption that the potential must take into account the effects beyond the α-cluster model. The experimental values of the ground- and excited-state energies and the ground-state r.m.s. radius are used to impose three restrictions on four parameters of the three-body potential. The remaining degree of freedom provides the one-parameter dependence of the width of the near-threshold 0^+_2 state and the $0^+_2 \to 0^+_1$ MTME, which are experimentally available. It should be emphasized that the determination of the parameters of $V_3(\rho)$ by fixing E_{gs}, E_r, and $R^{(1)}$ at the experimental values leads to a rather complicated dependence of Γ, M_{12}, and $R^{(2)}$ on the α-α interactions.

The calculations reveal that for all the two-body potentials under consideration Γ and M_{12} take values of about 16.5 eV and 9.0 fm^2 and become essentially independent of the choice of the three-body potential. At the same time, the excited-state r.m.s. radius $R^{(2)} \approx 3.9$ fm noticeably exceeds the ground-state r.m.s. radius $R^{(2)} = 2.47$ fm. Both Γ and M_{12} are well above the experimental data, which reflects a general trend for these values to be overestimated in calculations. Alternatively, for the two-body potentials corresponding to $\gamma > 6.35$ eV, *i.e.*, for the three-body potential with a strong attractive short-range term, both Γ and M_{12} decrease as the strength of the attractive term $|V_1|$ increases and its range b_1 decreases. The solutions of this kind optionally give the values of Γ and M_{12} which are surprisingly close to the experimental data. For these solutions, the excited-state structure undergoes a considerable modification by a strong short-range attractive potential, which entails a considerable amplification of the short-range component of the excited-state wave function and, hence, a decrease in the r.m.s. radius to unexpectedly small values $R^{(2)} \approx 2.8$ fm. Against intuition, the short-range component of the ground-state wave function decreases. In addition, the attractive short-range term of the three-body potential leads to the appearance of a narrow resonance above the 0^+_2 state.

In conclusion, a family of the effective potentials was found, which allows the experimental values for the basic characteristics of the ^{12}C(0^+) states, *i.e.*, E_{gs}, E_r, and $R^{(1)}$, to be reproduced within the framework of the α-cluster model. Concerning the fine characteristics, such as Γ, M_{12}, and $R^{(2)}$, the calculations reveal two principal choices of the effective potentials. For the first one, the calculated Γ and M_{12} are localized in small areas $\Gamma \approx 16 \pm 1$ eV and $M_{12} \approx 9 \pm 0.5$ fm^2, noticeably above the experimental data. In other words, if the size of the ground state is fixed, it imposes a stringent constraint on the finer properties, *i.e.*, Γ and M_{12} for quite arbitrary potentials. For the second one, with strong short-range attraction supporting an additional narrow resonance, both Γ and M_{12} take a wide range of values which might be chosen near the experimental data. These solutions exist if a narrow resonance is allowed; however, there are no experimental indications of a narrow resonance above the 0^+_2 state. The qualitative conclusion is that if E_{gs}, E_r, and $R^{(1)}$ are fixed at the experimental values, a considerable short-range component of the wave function is needed to improve the agreement with experiment for Γ and M_{12}. Certainly, the problem of a reliable description of Γ and M_{12} in the α-cluster model deserves a thorough investigation, *e.g.*, by using the nonlocal three-body potential describing the coupling with a twelve-nucleon channel at short distances.

References

1. E.E. Salpeter, Astrophys. J. **115**, 326 (1952).
2. F. Hoyle, Astrophys. J. Suppl. **1**, 121 (1954).
3. L.V. Grigorenko, R.C. Johnson, I.G. Mukha, I.J. Thomson, M.V. Zhukov, Phys. Rev. C **64**, 054002, (2001).
4. L.V. Grigorenko, M.V. Zhukov, Phys. Rev. C **68**, 054005 (2003).
5. H.O.U. Fynbo, Y. Prezado, U.C. Bergmann, M.J.G. Borge, P. Dendooven, W.X. Huang, J. Huikari, H. Jeppesen, P. Jones, B. Jonson, M. Meister, G. Nyman, K. Riisager, O. Tengblad, I.S. Vogelius, Y. Wang, L. Weissman, K. Wilhelmsen Rolander, J. Äystö, Phys. Rev. Lett. **91**, 082502 (2003).
6. O.I. Kartavtsev, Few-Body Syst. **34**, 39 (2004).
7. D.N.F. Dunbar, R.E. Pixley, W.A. Wenzel, W. Whaling, Phys. Rev. **92**, 649 (1953).
8. C.W. Cook, W.A. Fowler, C.C. Lauritsen, T. Lauritsen, Phys. Rev. **107**, 508 (1957).
9. M. Freer, A.H. Wuosmaa, R.R. Betts, D.J. Henderson, P. Wilt, R.W. Zurmühle, D.P. Balamuth, S. Barrow, D. Benton, Q. Li, Z. Liu, Y. Miao, Phys. Rev. C **49**, R1751 (1994).
10. A.G.W. Cameron, Astrophys. J. **130**, 916 (1959).
11. K. Nomoto, F.-K. Thielemann, S. Miyaji, Astron. Astrophys. **149**, 239 (1985).
12. K. Langanke, M. Wiescher, F.-K. Thielemann, Z. Phys. A **324**, 147 (1986).
13. I. Fushiki, D.Q. Lamb, Astrophys. J. **317**, 3621 (1987).
14. S. Schramm, Astrophys. J. **397**, 579 (1992).
15. Y. Funaki, A. Tohsaki, H. Horiuchi, P. Schuck, G. Röpke, Eur. Phys. J. A **24**, 368 (2005).
16. S.I. Fedotov, O.I. Kartavtsev, V.I. Kochkin, A.V. Malykh, Phys. Rev. C **70**, 014006 (2004).
17. D.V. Fedorov, A.S. Jensen, Phys. Lett. B **389**, 631 (1996).
18. N.N. Filikhin, Yad. Fiz. **63**, 1612 (2000).
19. S. Ali, A.R. Bodmer, Nucl. Phys. **80**, 99 (1966).
20. J.H. Macek, J. Phys. B **1**, 831 (1968).
21. F. Ajzenberg-Selove, Nucl. Phys. A **490**, 1 (1988).

22. F. Ajzenberg-Selove, Nucl. Phys. A **506**, 1 (1990).
23. W. Ruckstuhl, B. Aas, W. Beer, I. Beltrami, K. Bos, P.F.A. Goudsmit, H.J. Leisi, G. Strassner, A. Vacchi, F.W.N. De Boer, U. Kiebele, R. Weber, Nucl. Phys. A **430**, 685 (1984).
24. E.A.J.M. Offermann, L.S. Cardman, C.W. de Jager, H. Miska, C. de Vries, H. de Vries, Phys. Rev. C **44**, 1096 (1991).
25. W. Reuter, G. Fricke, K. Merle, H. Miska, Phys. Rev. C **26**, 806 (1982).